Analysis of Lepton Pair Production at GlueX

A thesis submitted in partial fulfillment of the requirements for the degree of

Bachelor of Science degree in Physics from the College of William and Mary

by

Jennifer Wang

Advisor: Justin R. Stevens

Senior Research Coordinator: Gina L.Hoatson

Date: May 9, 2017

Abstract

In this thesis, I investigated the isolation of electron/positron pairs that are produced from the interactions of a proton and photon and the decay of a heavy timelike photon in a process known as Timelike Compton Scattering. This is important in helping to understand the internal structure of the proton. We added restrictions onto the raw datasets in order to find events that represented a production of electron/positron pairs. We also found the statistical shape of background events, which do not produce electron/positron pairs, in order to remove the background noise in our selected events.

1 Introduction

An important problem in the field of nuclear physics is understanding the proton structure. There has been much progress toward this goal with new experiments and theoretical models [1]. One old, but powerful experimental technique for studying the internal structure of a material object (such as a proton) is scattering point-like particles on the object.

Now, scattering processes are important in understanding the quark and gluon structures of protons. We know that the proton is composed of quarks, with their own intrinsic spins. Curiously, the spin states of the quarks contribute very little to the proton's overall spin [1]. Newer experiments have pointed the this being a valence quark effect. The angular momentum from spin is shifted to orbital angular momentum, and orbital angular momentum from spin-orbit coupling may explain this strange proton spin phenomenon.

"The recently developed formalism by X. JI, A.V. Radyushkin, J.C. Colins ... of Generalized Parton Distributions (GPDs) showed that" we can learn more about what contributes to proton spin through experiments with hard exclusive leptoproduction experiments [6]. GPDs provide us with a framework

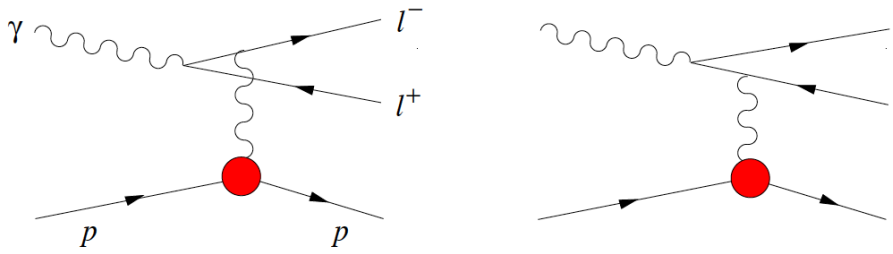

Figure 1: Feynman diagrams for the Bethe-Heitler Process

for characterizing hadronic structures with exact calculations. The simplest process that can be described in terms of GPDs is Deeply Virtual Compton Scattering (DVCS), $\gamma^* p \to \gamma p'$. Measurements of DVCS experiments have give us the imaginary part of the "Compton amplitude". The inverse process, $\gamma p \to \gamma^* p'$, is called Timelike Compton Scattering. This process gives us the real part of the "Compton amplitude", and in combination with the data from DVCS gives us constraints on models of GPDs [7].

In TCS, the incoming photon is real and interacts with a proton. The outgoing photon, γ^* is timelike, producing lepton pairs, e^+e^- in this instance. There is interference between TCS and the Bethe-Heitler (BH) process in which the incoming photon decays into a lepton pair first, and then the proton interacts with the leptons instead [7]. Feynman diagrams for the BH process are shown in Figure 1. Figure 2 is a Feynman diagram of the TCS process.

Other background events resemble TCS, the most significant of which is when a pion pair is produced, $\gamma p \to \pi^+\pi^- p'$, and the $\pi^\pm$ is mis-identified as $e^\pm$. Pion pair production occurs 10^4 times more often than $e^\pm$ pair production, and thus the signals representing these events need to be removed before analyzing the data.

There are also two benchmark processes. The first, $\gamma p \to J/\psi p' \to e^+e^- p'$, contributes $e^\pm$ pairs with invariant masses around $M_{J/\psi} = 3.097 GeV/c^2$. The

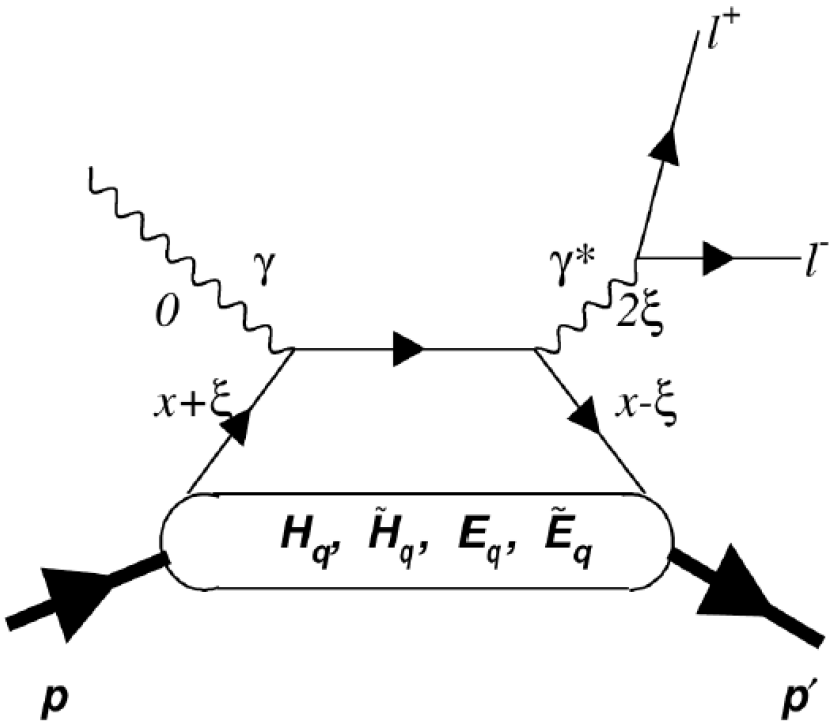

Figure 2: Feynman diagram of Timelike Compton Scattering. Everything in the top half of the diagram is calculable, and the GPDs H, $\tilde{H}$, E, and $\tilde{E}$ are what we want to find.

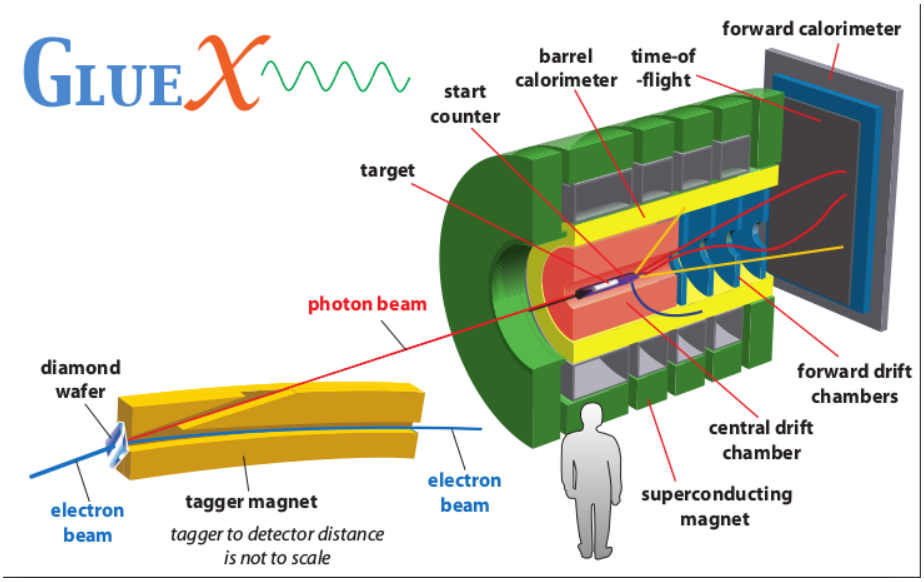

Figure 3: Diagram of the GlueX detector

second, $\gamma p \to \phi p' \to e^+e^-p'$, contributes $e^{\pm}$ pairs with lower invariant masses around $M_\phi = 1.012 GeV/c^2$. Recognizing these signature signals can help us confirm that our event selection process has removed the pion background.

2 GlueX Detector

The data for this analysis was collected during the spring of 2016 at Jefferson Lab. The GlueX detector was specifically designed for measuring photon-proton interactions. A schematic of the detector is shown in Figure 3.

Using the 12 GeV accelerator, a high-energy electron beam is produced and sent through a bremsstrahlung radiator. Coherent bremsstralung is a process in which the electron beam is passed through a diamond wafer; the electrons lose energy in the form of radiating photons. These resulting photons are linearly polarized and have an energy peak in the 8.2 GeV to 9.2 GeV range, as seen in Figure 4. The energy of the scattered electrons is measured in the tagger magnet

thus tagging the energy of the polarized photon. There are two instruments used to collect this information. The tagger microscope tags photons in the peak energy range, sampling at a finer resolution, while the tagger hodoscope tags photons with higher and lower energies using a wider resolution.

The photons travel into the GlueX detector where some will interact with a liquid hydrogen target. The radially symmetric detector layers are then able to measure the paths and charges of the resulting particle shower.

The solenoid magnet around the entire detector produces a magnetic field of 2T in the direction of the photon beam. A central drift chamber (CDC), based on straw-tube technology, can provide information on the paths of any charged particles. The forward drift chamber (FDC) also helps measure paths of charged particles. Around the CDC is a barrel calorimeter (BCAL). The BCAL measures the energy of particles that deflect from $11^o - 126^o$, using silicon photomultipliers. The forward calorimeter (FCAL), located down the end of the track, also measures particle energy for particles that only deflect up to 11^o. Only $e^{\pm}$ and photons will deposit all of their energy in the calorimeters; the calorimeters will measure a fraction of the energy of other particles. A time-of-flight wall (TOF), also located at the end of the track, gives timing information.

The information from the drift chambers can give an accurate reconstruction of the path of a particle. The length of this path, combined with the measured time of flight, allows the velocity to be calculated.

The energy of the all the particles measured allows us to calculate their masses. The collected data can also be use to calculate the 4-momentum of every particle. As we also know the energy and masses of the starting photon and proton, we have a redundancy check to make sure the initial and final four momenta are consistent. The difference in these values is termed the missing

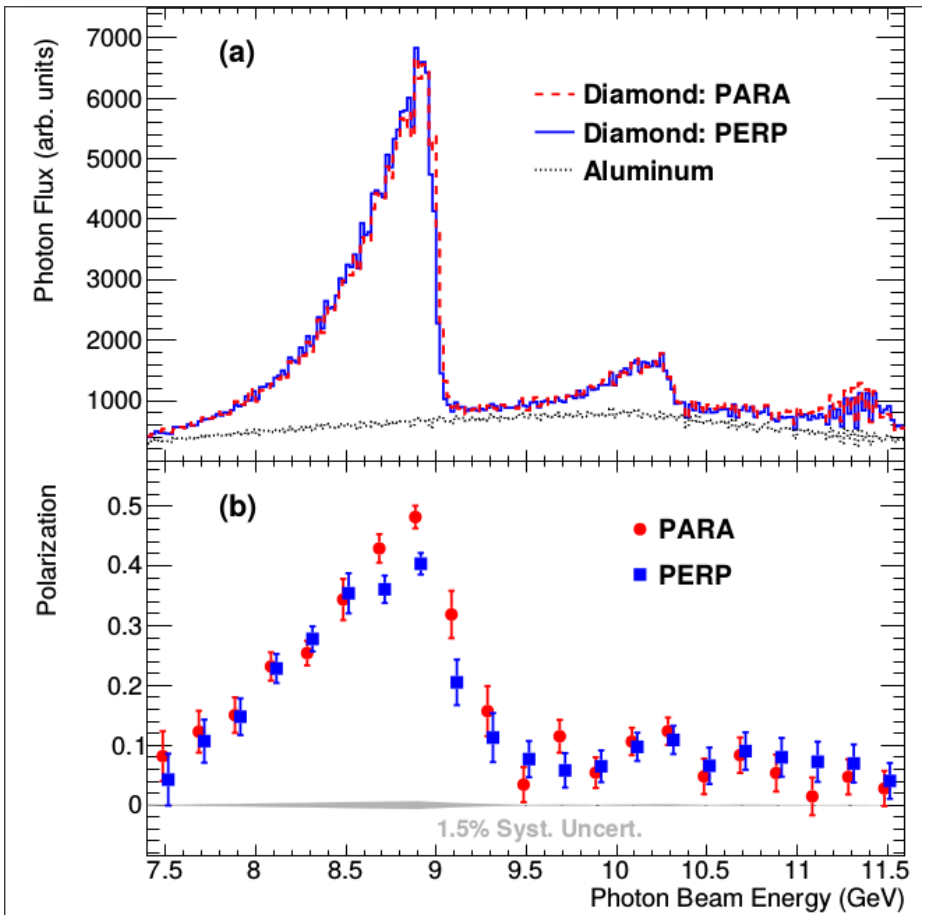

Figure 4: (a) The intensity of photons of different energies produced via bremsstrahlung with the diamond in different orientations. (b) The polarization of photons produced via bremsstrahlung

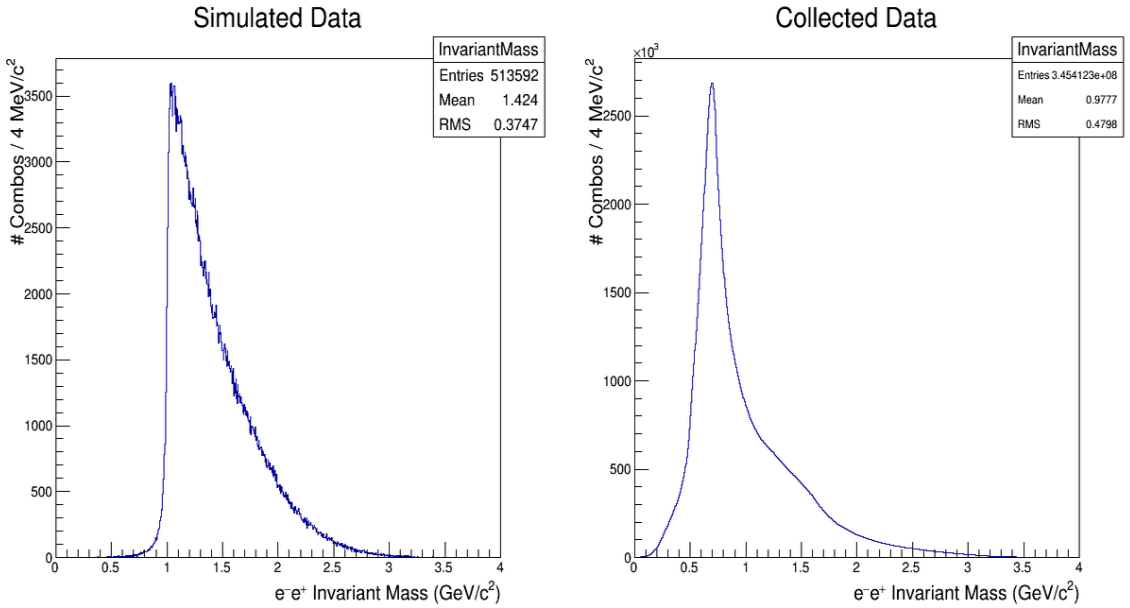

Figure 5: Invariant mass plots for simulated data on the left and raw collected data on the right

mass.

3 Event Selection

3.1 Event Combination Selection

I have applied cuts within the data to try to restrict the events we select for analysis to only those that correspond to the production of $e^{\pm}$ pairs. I first used a simulation of the TCS process just to confirm a shape for the distribution of masses. The data set only simulated the TCS process, and the results for this lack the background noise signal from the pions or benchmark processes. This is shown in Figure 5 on the left.

The requirements below follow from the constraints and restrictions of the experimental setup.

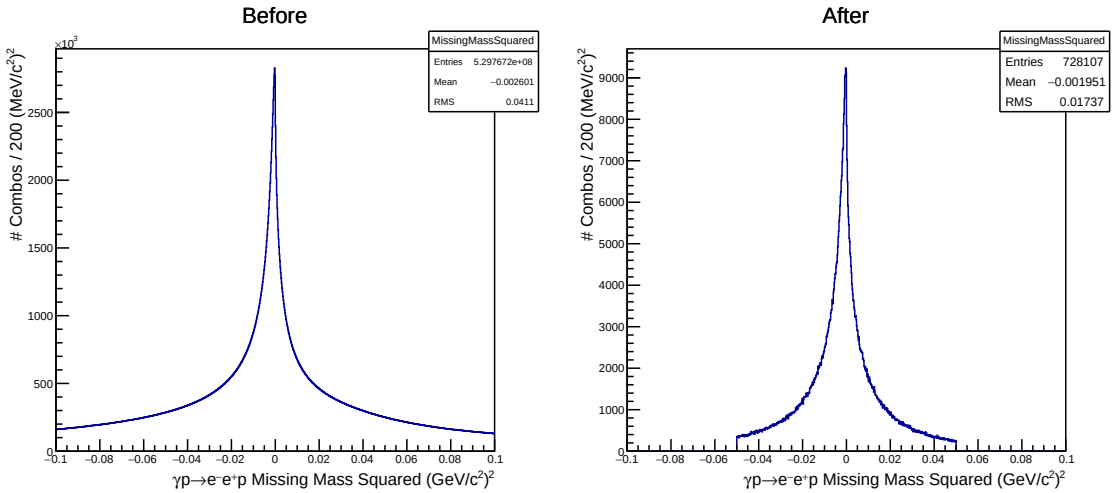

Figure 6: The frequency distribution of missing mass before and after the missing mass squared and kinematic fit cuts

Requirements:

- Missing Mass Squared: $|MM^2| < 0.05 GeV^2$
- Kinematic fit: $p > 5 \times 10^{-7}$
- Beam Energy: $6.0 < E_\gamma < 12.0 GeV$
- $e^{\pm}$ Energy/Momentum: $E/p > 0.8\ GeV/c^2$

Because of the redundancy check on the initial and final masses, we expect our missing mass to be zero. As experimental errors still occur, we allow the value of our missing mass to be nonzero but small. We can also check that the momentums of all the particles add up. The kinematic fit is a measure of how well the 4-momenta in the data is conserved. This metric uses a χ^2 test, and we preferentially want to keep events with a relatively high confidence level, in this case anything greater than 5×10^{-7}. Figure 6 shows us the distribution of missing mass when these cuts are placed.

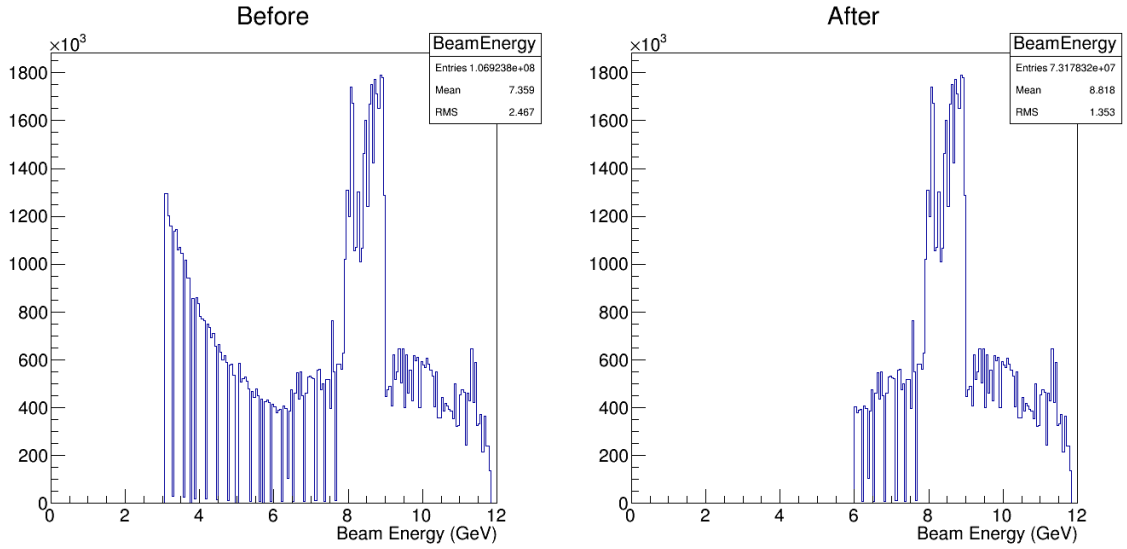

Figure 7: The distribution of beam energy before and after the beam energy cut is applied

We know that the energy of the electrons used to produce the photon beam had energies around 12 GeV, so the maximum energy of the incoming photons is 12 GeV. However, theoretically, the alignment and placement of the diamond wafer produces coherent bremsstrahlung in the 8.4 - 9.0 GeV range, giving us a spike in the number of photons in this range. We also only want the high energy photons, and therefore we place the lower energy bound at 6.0 GeV. Figure 6 shows this cut placement, and the expected peak. There is an odd anomaly around 8.0 GeV, and this arises from the difference in sampling size of the hodoscope and the microscope as this is the boundary where one begins detection and the other stops.

Finally, we know the electrons will have an energy-to-momentum ratio near unity because the simulated data set gives this to us in Figure 8. The pions will have lower ratios because they only deposit some of their energy in the BCAL and FCAL, so we applied a cut to remove any events producing particles with

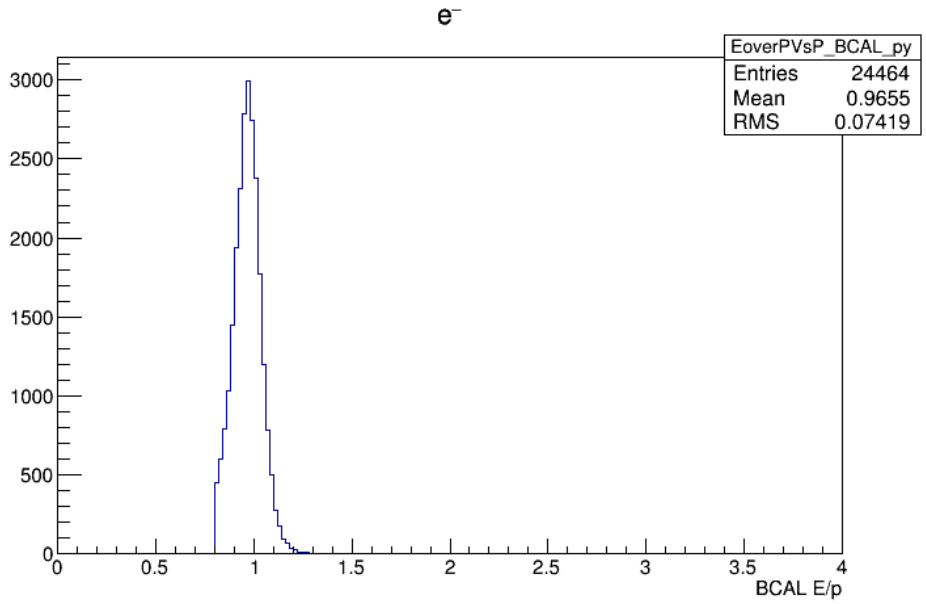

Figure 8: The distribution of electrons in the simulated data

$E/p < 0.8GeV/c^2$. The result of this is shown in Figure 9.

The final invariant mass distribution we see in Figure 10 still has background noise. We assume this comes mostly from pion-producing events. We do notice a peak at about $3GeV$ where we expect the J/ψ process to contribute. This indicates that we are on the right track in isolating the electron/positron signal.

3.2 Background Event Selection

Statistically, because the production of pion pairs occurs so much more frequently than the production of $e^{\pm}$ pairs, there will be a greater proportion of pion background noise when we select for electrons than electron background when we select for pions. Therefore we can isolate the shape of the pion background. Then we can remove it from the first event selection.

If all the other cuts are kept the same, but the energy-to-momentum ratio is required to be less than 0.8GeV, we theoretically get only pions. The invariant

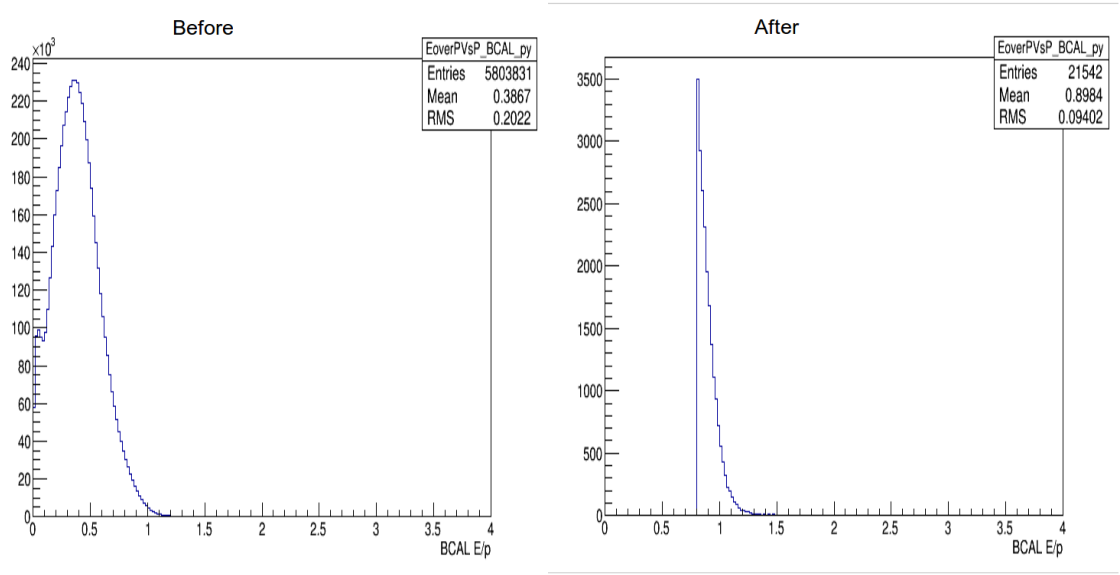

Figure 9: The E/p distribution of electrons before (left) and after (right) the E/p cut

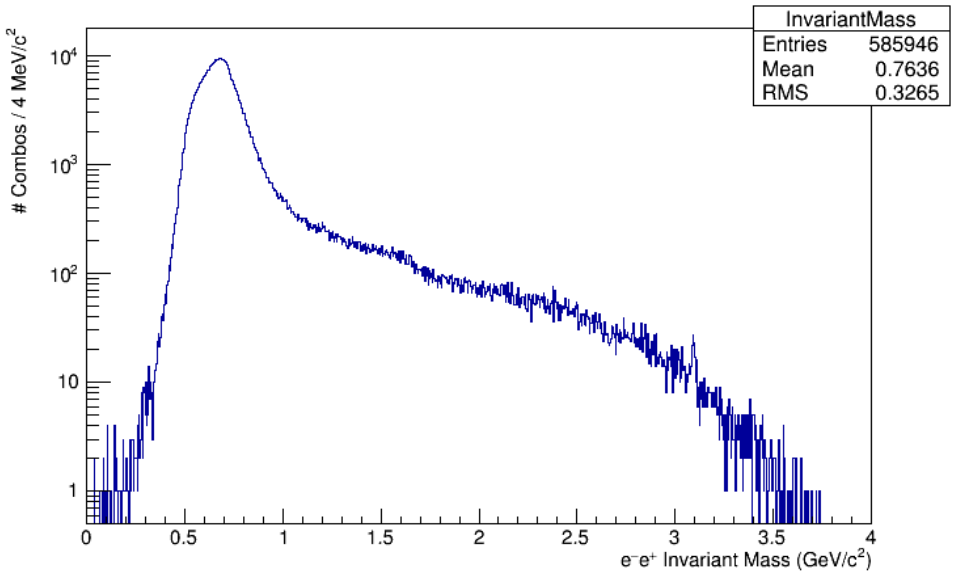

Figure 10: The invariant mass distribution on a log scale

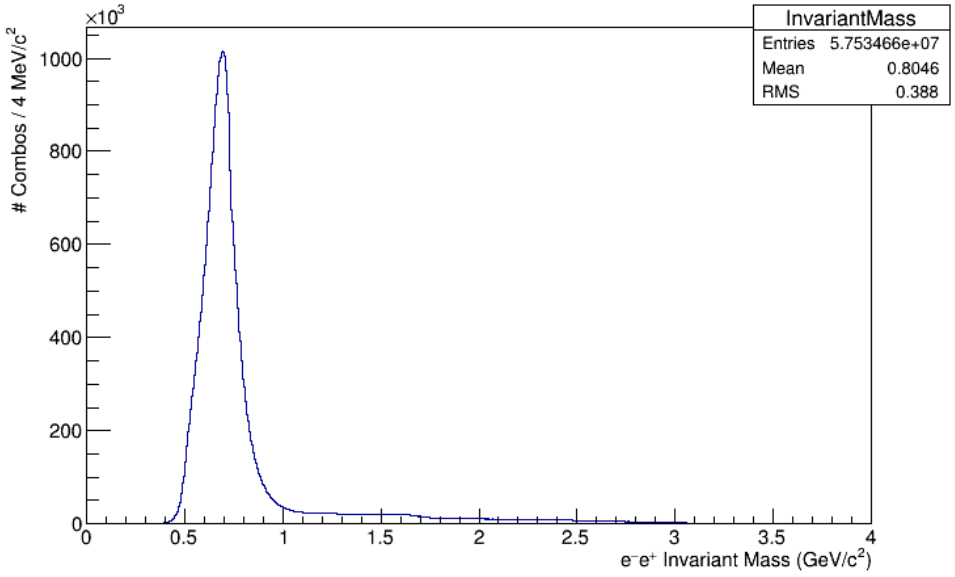

Figure 11: Invariant mass distribution of the pion selection

mass distribution for this is shown in Figure 11. Figure 12 shows the same plot on a log scale that can be compared with Figure 10 from the first event selection.

If the distribution of pion masses is scaled and normalized, it can be removed from the first event selection to hopefully give us an invariant mass distribution that more closely resembles the simulation.

4 Summary, Conclusions and Outlook

We first found the events in the data that appear to produce $e^{\pm}$ pairs, and then we isolated the background $\pi^{\pm}$ producing events. After normalization of these background events, their shape can be removed from the first event selection. In the future, someone will remove the J/ψ and the ϕ processes and separate the TCS events from the BH ones. Once only the TCS events are left, the data can be analyzed to compare it to the GPD models.

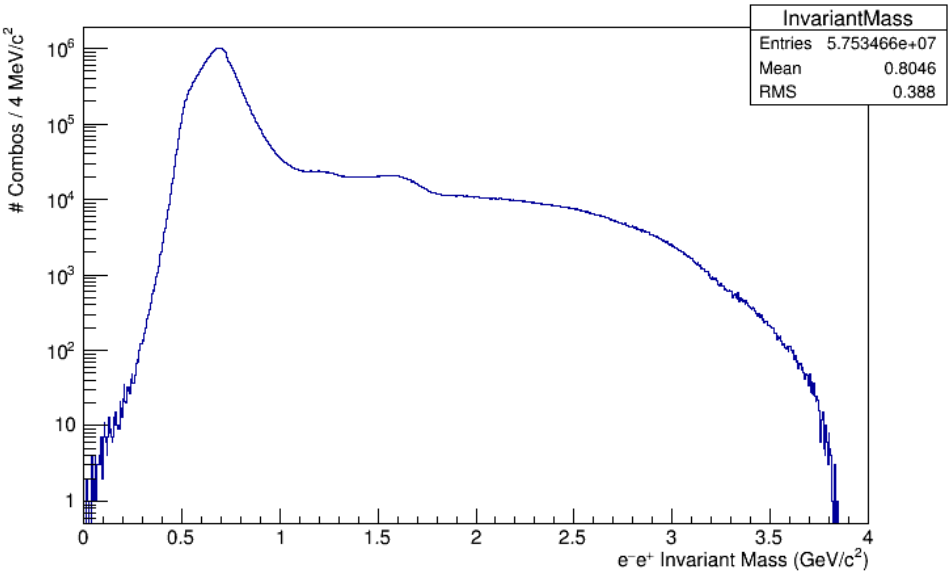

Figure 12: Invariant mass distribution of the pion selection on a log scale

References

[1] Aidala, C. A., Bass, S. D., Hasch, D., & Mallot, G. K. (2013). The spin structure of the nucleon. Reviews of Modern Physics, 85(2) doi:10.1103/RevModPhys.85.655

[2] Bergera, E. R., Diehlb, M., & Pire, B. (2001). Timelike compton scattering: Exclusive photoproduction of lepton pairs.

[3] GlueX Collaboration. (2015). First results from the GlueX experiment. AIP Conference Proceedings, 1735(1) doi:10.1063/1.4949369

[4] Goritschig, A. T., Pire, B., & Wagner, J. (2014). Timelike compton scattering with a linearly polarized photon beam. Physical Review, 89 doi:10.1103/PhysRevD.89.094031

[5] Leverington, B. D. (2010). The GlueX lead-scintillating fibre electromagnetic calorimeter. (Unpublished PhD). University of Regina

[6] Paremuzyan, R. (2010). Timelike compton scattering. Yerevan Physics Institute

[7] Pire, B., Szymanowski, L., & Wagner, J. (2009). Timelike compton scattering in ultraperipheral collisions. Proceedings of DIS

[8] Senderovich, I. (2012). A polarized high-energy photon beam for production of exotic mesons. (Unpublished PhD). University of Connecticut